Exploring the Use of Desktop 3D Printing for Microfluidics Prototyping

Exploring the Use of Desktop 3D Printing for Microfluidics Prototyping

Peter Garone

Thesis in the Field of Biotechnology for

the Degree of Master of Liberal Arts in Extension Studies

Harvard University

May 2017

Abstract

Despite the tremendous impact of 3D printing on mechanical and design prototypes the use of 3D printers in microfluidics has been extremely limited. The current methods of constructing microfluidic devices use relatively complex, multistep processes that require the construction of molds (soft lithography) or photomasks (IC style and paper microfluidics). 3D printing has the potential to create microfluidic devices in a single step- dramatically reducing the time from design to the completion of a working prototype, as well as avoiding the large overhead cost associated with a large scale manufacturing process.

This work takes a close look at the use of one method of 3D printing called Fused Filament Manufacturing (FFM) to create microfluidic prototypes. This work investigates the barriers that have prevented the wider use of this method in microfluidics and how these barriers may be overcome. The components of this study include a look at the design of microfluidic devices for 3D printing, the resolution and design limitations of 3D printing using FFM, and the printing of basic microfluidic components.

Finally, as an example of using 3D printing for microfluidics, a prototype device that could be used to detect Sarin gas (a nerve agent) in blood is designed and constructed.

Acknowledgements

First off I'd like to thank my wife Debbie who put up with the expenses and time commitments associated with her husband's pursuit of a mid-life crisis degree.

Thanks also to friends who were interested in this pursuit and offered encouragement along the way.

Thanks also to Dr. Vaughn and Dr. Denkins who gave me guidance and encouragement along the way and to Dr. Yang who graciously agreed to oversee my thesis project.

And lastly I am very thankful for the excellent instruction, enthusiasm, and dedication of all the professors who taught the courses I took over the years at the Extension school.

Table of Contents

List of Figures

Chapter 1

Introduction

Despite the tremendous impact of 3D printing on mechanical and design prototypes the use of 3D printers in microfluidics has been extremely limited. The current methods of constructing microfluidic devices use relatively complex, multistep processes that require the construction of molds (soft lithography) or photomasks (IC style and paper microfluidics). 3D printing has the potential to create microfluidic devices in a single step- dramatically reducing the time from design to the completion of a working prototype, as well as avoiding the large overhead cost associated with a large scale manufacturing process. Despite these advantages the use of 3D printing in microfluidics has been very limited.

A desktop 3D printer (Lulzbot Mini) which uses Fused Filament Manufacturing (FFM) to create microfluidic prototypes was used to investigate the use of 3D printing for microfluidic prototypes, to see what barriers that have prevented the wider use of this method in microfluidics, and how these barriers may be overcome. The components of this study will include a look at the design of microfluidic devices for 3D printing, the resolution and design limitations of 3D printing using FFM, the printing of basic microfluidic components, and the suitability of available FFM materials for microfluidic applications.

Finally, as an example of using 3D printing for microfluidics, a prototype device that could be used to detect Sarin gas (a nerve agent) in blood will be designed and

constructed. A portable unit that can be used to determine the extent of exposure to Sarin gas could help prioritize the care delivery and inform the response team as to the nature of the emergency (Sarin gas detected).

Microfluidics and biological applications

Microfluidics (fluidics on the micron->mm scale) has been an area of major research and investment in the biotechnology field. The small size of microfluidics devices lends itself to manipulating the small sample sizes typically encountered with biological samples. The small size also reduces the cost of reagents, disposal costs, and can minimize the "dead space" in the device which might lead to cross contamination. If the devices can be produced cheaply enough they could be used for a single use, which has advantages in many applications[i] (Streets 2013).

Microfluidic devices have predominantly been made using either integrated circuit based processing, which has excellent resolution (down into the nm range) and highly automated processing equipment or a hybrid process called soft lithography which uses a replica molding technique to form layers of PDMS that can be joined together or fused to other materials[ii] (Whitesides 2001). Both of these are multistep processes that can be quite complex and expensive.

More recently simple, low cost microfluidics devices have been constructed using paper which has a very low material cost but is limited to a 2D structure and may not be compatible with a large number of chemistries[iii] (Martinez 2007).

3D Printing

3D printing has revolutionized mechanical design. 3D printing accelerates the design process by enabling the rapid construction of prototypes before committing the design to the full manufacturing process [iv] (Hiemenz 2014). The ability to rapidly iterate the design before manufacturing has been a great boon to the machine and design community.

By virtue of the layer by layer construction employed by 3D printers, complex shapes can be formed in a single step print process, which would require a complex multi-step manufacturing process with other fabrication. The ability to quickly design and build a structure optimized for a single purpose opens up new possibilities. For example a specialized microfluidic device could be designed and built for one experiment, whereas the construction of that device by other means would not be feasible due to time and/or cost.

The price of 3D printers has come down to the point where they don't cost a whole lot more than a desktop computer or printer. Coupled with open source or academic priced 3D design software the ability to design and create complex microfluidic devices using a 3D printer quickly and inexpensively is now possible.

By means of comparison the equipment required for an integrated circuit based process will cost at a minimum several million dollars and will require mask costs for each new device on the order of $30k or more, depending on the resolution of the features required for that device. Once the masks are made the production cycle time is typically in the range of 6-10 weeks, depending on the device complexity. In addition, because of the diversity of microfluidic applications it is typically necessary to create a

unique or modified process to fabricate each new device, which adds to the time needed to produce a working prototype. Once large scale production of a device commences these large up-front costs can be amortized over many parts but the sizeable upfront investments present a large barrier to design and validation of a new microfluidics product.

3D printing can be done by several different methods which all share a common layer by layer construction of the printed object. Briefly these include:

1. Stereo Lithography (SLA) – UV patterning of a photo resin to build up the 3D object. After each layer is patterned the object is drawn up out of the bath of photo resin to position if for the next layer patterning.
2. Inkjet (polyjet) technology- layers of particles are rolled onto a surface and a liquid binder is sprayed in the desired pattern, forming the final structure. The unbound particles are removed at the end of the process.
3. Selective laser sintering (SLS)- similar to inkjet printing in that layers of particles are rolled onto a surface except that the particles are fused together using a high power laser (eg. CO_2 or Nd:YAG).
4. Laminated Object Manufacturing (LOM)- Layers (sheets) of material such as paper, plastic, or metal are laid down and material is ablated (removed) to form a pattern using a CO_2 laser. After one sheet is patterned the next is laid on top and the process is repeated.
5. Fused filament manufacturing (FFM) (a.k.a.- FDM: fused deposition modelling) - Filaments of thermoplastic material are fed into a heated nozzle, which melts the

filament. The melted material is extruded thru the nozzle to form the part, layer by layer. This is the method selected for this work.

A more detailed comparison of the different methods of 3D printing is given by Gross et. al[v] (Gross 2014).

FFM printing was chosen for this study for a number of reasons. First, there is a wide array of inexpensive materials available for fabrication with FFM that are compatible with the classes of chemical used in microfluidics[vi] (Waldbaur 2011). The FFM process also does not involve harmful chemicals or exhaust so it can be set up and run in a home or office environment, literally on a desktop. There is also a greater number of manufacturers of these type of printers, which gives a greater choice in equipment and a larger eco-system of supplies and material.

Overview of the 3D design and printing process

A brief overview of the process beginning with the design of a 3D microfluidic device to its construction using 3D printing (using FFM), will help highlight the primary considerations in the design and construction of microfluidic devices using this technique.

The first step is to design the microfluidic device using 3D design software. Once the design is complete the file must be converted to a format that can be used to construct a layer by layer model of the device, which will be used by the 3D printer to build up the 3D device. The “slicer” software used to do this will also control the path of the extruder nozzle of the 3D printer as it builds up the layer using a thread of molten fiber. The slicer software also controls the temperature of the nozzle, the filament push and pull rates

(forming the thread and breaking the thread), and the speed of travel of the print nozzle. The slicer software also specifies the thickness of the object surfaces (solid portion) and sets up the internal fill of the device. A typical 3D printed part will not be completely solid, but rather will contain internal supports. The reasons for this are two-fold, saving material costs and reducing the print time.

When the printing begins a heated nozzle is used to melt the filament and a drive mechanism is used to extrude a fine thread of molten material through the nozzle. Pushing the filament extrudes the thread, retracting the filament causes the thread to terminate (break off). As the thread is alternately being formed and broken, motors drive the nozzle in the x and y dimensions (horizontal) in a pattern determined by the slicer software. As each layer (slice) is complete the nozzle is stepped up in the z axis (vertical) to begin the next layer. Thus the 3D object is printed layer by layer. Because each subsequent layer rests on the previous layer, care must be taken to ensure that there is sufficient support during the build. Insufficient support can lead to a huge mess as the structure collapses and the molten thread is sprayed into empty space (take my word for it).

3D printing is a completely additive process, compared with integrated circuit style processing and soft lithography, where material is both added and etched away (removed) to form the device structure.

Previous use of FFM 3D printers for microfluidic applications

The first reference to the application of FFM 3D printing in the manufacture of microfluidic devices that I could find was by Wang et al in 2001[vii] (Wang 2001). They were principally concerned with modeling pressure driven fluid flow with some simple structures printed using FDM. Their study was hampered (terminated) by leaks and deposition artifacts that interfered with their fluid flow modeling. The surface roughness of the FFM printed channels also contributed to the failure of their fluidic modeling to predict experimental results (which they didn't even bother to show). While the difficulty in accurately modeling the fluid flow due to surface roughness is not something that will be addressed in this work, ensuring that the microfluidic structures do not have leaks is essential to the use of FFM 3D printing for this application. Careful study of the printer settings will be taken to address this issue.

More recently several groups have used FFM 3D printing to create microfluidic devices. Bishop et. al.[viii] printed some simple microfluidic devices including a Y-shaped mixing channel used to prepare Prussian blue nanoparticles (Bishop 2015). They also printed some threaded fittings for connections of the devices to hoses. The Prussian blue nanoparticles act as a catalyst for the reduction of hydrogen peroxide (H_2O_2) on a gold electrode. The Prussian blue nanoparticles formed in a 3D printed microfluidic mixer were coated onto gold electrodes and then incorporated into a second 3D printed devices used to measure the molarity of H_2O_2 in solution.

Kitson et al[ix] recently created some simple multi-chamber chemical "reactionware" devices that used rotation of the device to initiate gravity flow of the liquids from one reaction chamber to the next (Kitson 2013). To illustrate the utility of

such a design they constructed a reactionware device to perform a commonly used 3 step organic reaction sequence.

1. Diels–Alder cyclization, a C–C bond forming reaction
2. Formation of an imine
3. Hydrogenation of the imine to the corresponding secondary amine

This study focused on very simple devices which did not demonstrate the utility of using 3D printing to prototype more complex microfluidic devices but did present a clever method to control a chemical reaction sequence by rotating the device to initiate different steps of a chemical process.

Sarin, a chemical warfare agent

Sarin ((RS)-Propan-2-isopropyl methyl phosphonofluoridate) is a clear colorless liquid that is easily volatilized. It is one of the most toxic chemical warfare agents. It was used in the 1994 Tokyo subway attack and again in Syria during the civil war.

Sarin works on the nervous system by blocking the enzyme AChE (acetylcholine Enzyme), which is used to break down the neurotransmitter acetylecholine. When AChE is blocked acetylcholine will build up in the synapses of the nerves and continue to stimulate the firing of the neurons. This will lead to seizures, convulsions, paralysis, and death by asphyxiation.

The ability to quickly measure the level of sarin exposure of individuals in a terrorist attack would enable the first responders to prioritize the treatment of the victims.

As a demonstration the utility of 3D printing in microfluidic prototyping the design and fabrication of a microfluidic device that could be used to detect Sarin gas in blood samples was undertake. This device utilizes the “reaction-ware” concept to initiate the different chemical steps used in the detection method. A similar devices was originally constructed using a multi-step soft lithography process.

Chapter 2

Materials and Methods

This project had 3 main objectives:

1. Study the design of microfluidic devices for 3D printing, including the resolution (minimum printable feature size), design limitations, and material
2. Considerations (print and chemical compatibility) using FFM 3D printing for microfluidic applications.
3. Construct and evaluate the design of the basic microfluidic components including channels, mixers, reaction chambers (cavities), reservoirs (inlets), outlets, and connectors (hose barbs and threaded connectors) constructed with FFM 3D printing.
4. Construct a prototype microfluidic device using 3D printing as an example. The particular device will be a prototype for analyzing a blood sample to detect the exposure to Sarin gas (a nerve agent).

Design considerations and constraints

To investigate the fabrication of microfluidic devices I used an inexpensive ($1250) desktop FFM 3D printer – the Lulzbot Mini (Figure 1).

General comments on software for 3D printing

First off, using a PC, instead of a Mac will make life much easier when it comes to 3D design and printing. There are many more applications available for the PC and these are of much higher quality as well. Do yourself a favor and get a PC, if you don't already have one, if you're interested in 3D printing.

Designing in 3D is much more complicated than design in 2D. Ensuring that the various 3D objects are aligned properly, with no gaps can be cumbersome and time consuming. Checking the design from different vantage points and measuring the lengths and angles is necessary to avoid errors. There is a steep learning curve learning to use this software. I did not do an exhaustive examination of the different software programs but in general each has an underlying design methodology on how to create a 3D drawing. Your 3D design will be much easier if you adapt to the methodology envisioned by the software designers.

I tried several "freeware" 3D design programs and they work OK (on the PC) but are lacking in ease of use. There is good academic pricing for some of the software packages, which is good since these programs are very expensive. The 2 best choices seemed to be SolidWorks and Autodesk's Inventor (which I used).

For the slicer software the Open Source software is used for the majority of the FFM printers. My printer came with a version of Cura specifically tailored to the Lulzbot, but in the end I found that another open source program called Mattercontrol provided more control over the various print parameters and had the capability to show the details of the individual layers (slices) that the print is built up from. This capability was very helpful in understanding why some designs printed more successfully than others.

"Lego" 3D design software

Increasing the ease of use for 3D design software would be a big help towards a wider adoption of 3D printing for microfluidics. Perhaps a "Lego-like" approach where pieces are selected from a library of standard microfluidic components which then can be "snapped" together to build a device.

AutoCAD Inventor partially fulfills this goal. Individual parts can be drawn and saved. These parts can then be joined together in an assembly. Unfortunately without being able to parameterize different dimensions (length, tube ID, wall thickness,…) the size of the part libraries needed create a designs with many different dimensions would be unwieldy.

Structure supports and adhesion to the print bed

With FFM supports are needed to hold up structures as they are being built. A cantilever cannot extend off an object without a support being printed underneath. I had several instances where a print failed because there was insufficient support so it is desirable to consider how the print is built up layer by layer to ensure that there will be sufficient support for each layer. Once one section fails the printer will continue to try to build on top of it, spraying molten thread into thin air.

One solution is to have a second nozzle printing support material that can be dissolved away. There are some combinations of materials that can utilize this approach. I didn't try this because my printer only has one nozzle, as do most (relatively) inexpensive printers so I can't verify that this approach is without its own limitations.

The slicer software does allow for automated support generation. Auto-generated support should be carefully examined to ensure that the supports will actually be sufficient or don't ruin the functionality of the device.

As a test case auto generated supports were used for a simple "Time to Drain" structure (see Figure 2A). The software drew supports underneath the inlet basin and at the base of the angled tube, but not along the length of the tube. This can be seen in the 2D view of the first print slice (Figure 2B). The subsequent print failed (Figure 2C) because the base was not sufficient to support the angled tube.

Partially drawing the support (support drawn under the angled tube) led to a successful print as did a fully drawn support (see Figure 3).

In another case using auto generated supports, internal supports were added, which closed down the channels of one of the microfluidic devices. This can be avoided in the software settings but shows that auto-generated supports should be checked before committing the design to print to make sure they provide sufficient support or that the support does not lead to unexpected problems.

Alternate Design Methodology

The 3D design is the most labor intensive part of the process of creating microfluidic device prototypes with 3D printing. Simplifying the design process would go a long way to making the use of 3D printing more widely used in microfluidics.

An alternative design methodology, to save on design time at the expense of print time and materials, is to design the channels and chambers of the microfluidic device as a solid and then subtract this from an enclosing cube. This makes the focus of the design the actual channels and chambers of the device, rather than the walls surrounding those

chambers. With the standard design flow the surrounding elements can obscure the fluid elements, necessitating multiple cross sections to verify the internal structure is correct.

An example of this technique used to draw a simple Time to Drain structure is shown in Figure 4. As mentioned, though the design effort using this technique was reduced the print time for this particular structure took over 2X longer, 8 hours 12 minutes vs. 3 hours 44 minutes (the drawing of the equivalent device is shown in Figure 3).

For a more complex device the enclosing cube might need to be replaced by a more complex enclosure.

Drawing the tubes and chambers of the device does make it easier to visualize and verify the device, as opposed to drawing the structures that contain the fluid channels and chambers. This method could be very helpful in complex designs.

Structural limitations of 3D prints

In order for the FFM 3D print to be successful the device must be firmly connected to the platform as well as the previous, underlying layers. The printer can't print into thin air, there needs to be underlying structural support for each layer of the print.

This need for support can limit the steepness of the angle of an outward directed object. Some more expensive printers get around this by having a second nozzle that can be used to print supports which are later dissolved or etched away. This experimenter didn't have that luxury.

The support must also be solid, if it is too flimsy the structure will collapse during printing and make a big mess. Though this will not be explored in detail, early failures have pointed out the need to address this.

For a successful build it is essential to think through how the device is built up to ensure there is sufficient support for of the device. It may be that the device could be printed more successfully lying on its side or even upside down. The ability to look at the layer by layer construction slices with MatterControl was very helpful for figuring out why a print failed or for checking the support structure, especially for auto-created supports.

In integrated circuit manufacturing design rules, along with design rule checkers, have been implemented to ensure that designed structures can be manufactured successfully. A similar set of design rules would be a help for the successful design of microfluidic structures. A first attempt to formulate a set of design rules, specific to the Lulzbot mini printer and more generally to FFM follows. Note that the specific dimensions may be dependent on the build material, the nozzle size and the print stage preparation.

Rules:

Minimum base contact area – 4 mm^2

Maximum aspect ratio (when base contact below a given area) – 5:1

Maximum size (x,y) – 152 mm

Maximum height (z) – 158 mm

No cantilevers

Minimum angle for an unsupported sloped object - 30°

Minimum opening size – 1 mm

Minimum wall thickness – 2 mm

The exact dimensions of these rules would be determined by a series of test structures, to verify which ones print successfully and which ones don't. The numbers given here represent estimates based on my experience gained during the course of this work.

Investigation of the resolution and other print capabilities

The stated resolution of a 3D printer actually refers to the layer thickness that the part is built up with. The layer thickness is not equivalent to the minimum channel size that one can print and only refers to the z – axis. The x and y dimensions are limited by the nozzle width, the precision of the print head controller, and the variance in starting and stopping of the printing at the edges of the printed objects.

Using the 0.5mm nozzle that comes with the Lulzbot Mini, resolution structures with square channel sizes ranging from 3mm to 1mm in 0.5mm steps were printed in horizontal, vertical, 15°, and 45° orientations using a 0.5mm nozzle. Close examination shows that the 1mm tubes were barely open for all orientations (Figure 5A). The vertically printed tubes were better defined. There was evidence of the plastic thread sagging from the top of the other tubes due to gravity. In practice the 1mm tubes did not consistently work (closed off somewhere along the tube) and the 1.5mm tubes had a much slower and more erratic flow rate than that observed with tubes 2mm and above.

Other nozzle sizes are available for the FFM printers and the minimum size I was able to find was 0.25mm, meaning the thread extruded from the print head should have a

diameter of half that of the 0.5mm nozzle. The minimum size tube I was able to resolve with the 0.25mm nozzle dropped to 0.75mm (Figure 5B) and a 900um x 900um Time to Drain structure was successfully printed and verified to function.

The cost for using a smaller nozzle size is that the print time takes longer. The print time for the Time to Drain structure increased from 3hr 6min to 4hr 37min when going from a 0.5mm nozzle to a 0.25mm nozzle. Depending on the resolution requirements this extra print time may be worthwhile.

Eliminating microchannel Leakage

One of the first papers reporting the use of FFM 3D printers for microchannels reported problems with leaking. They attributed this to small gaps between the threads that make up the 3D printed structure. This problem was also observed with some of my early printed structures.

To understand this problem it important to consider that a 3D printed part is not a completely solid object. To save time and material the outlines of the structure is printed with a solid shell thickness, which is defined in the slicing software, while the interior of the part uses an open fill pattern (waffle or hexagonal) to provide support. Looking at the slices that build up the part which leaked it was observed that there were places where the tube wall thickness was only a single thread of material. This occurred when I used a wall thickness of 1mm, which means that with a 0.5mm nozzle the wall thickness consisted of at most used 2 threads of material. When the microchannels made turns the wall thickness was reduced to a single thread of material in places. The leaks did seem to be coming from these areas.

Changing the settings to use a thicker 2mm shell thickness eliminated the leaking problem (4 threads of material surround the channels with a 0.5mm nozzle).

Material considerations

One of the compelling reasons for choosing an FFM style 3D printer over other methods of 3D printing is the wide range of filament materials available. This gives a lot of choices in terms of chemical compatibility and other physical properties like optical transmission so that an optimal build material can be selected for a particular application. There are even semi-metallic filaments available that are electrically conductive.

Chemical resistance

Chemical resistance of the different 3D printing materials is important to consider for the particular application. There are many guides available that give great detail on the chemical compatibility of different plastics to different chemicals. Overall the most versatile material chemically is polypropylene but the best material to use will depend on the particular chemicals used in the application.

Despite the wide array of filament materials available it is likely that other materials, like glass, filter material or coated beads may be useful to incorporate into a device. Glass was integrated into the design of the sarin detection microfluidic device described later.

Optical/EM transmission (integration with spectrophotometers)

Using spectroscopy to analyze the extent of reactions occurring or identifying the chemical components present is a common tool in chemistry and biology. The common plastics used as FFM materials are generally transparent in the visible spectrum and part of the near infra-red. An example absorption spectrum is shown in Figure 6. It shows that polypropylene is transparent from 400nm to about 1100nm before different absorption peaks associated with the chemical bonds kick in. Unfortunately the a characteristic ribbed structure of FFM prints, which results from the layering of the polymer threads, tends to scatter light and make the material opaque. This suggests that use of a glass viewing port would be desirable for such applications. Glass ports were used as optical viewports and to seal chambers where different chemicals were loaded into the sarin detector microfluidic device prototype.

Surface modifications (like PDMS)

One of the benefits of using PDMS to construct microfluidic devices is the ability to chemically modify the surface properties of PDMS. For example Khorasani et al modified the surface of PDMS using a pulsed CO2 laser to introduce peroxide groups[x] (Khorasani 1999). They used the peroxide groups to polymerize 2-hydroyethyl methacrylate and significantly reduce blood platelet adhesion.

I did a limited literature search and found a few mentions of surface modification by plasma or UV exposure but did not see any applications for FFM materials. Time limits excluded doing much more.

Comparing 3D printing to other methods of Fabricating Microfluidic devices

A brief comparison between 3D printing using FFM to other methods commonly used to create microfluidic devices was going to be made, but Waldbaur et. al. have already done this so I just refer you to their work (reference iii, Table 2).

Chapter 3

Results

This section describes the construction of the individual microfluidic elements followed by an example of a complete microfluidic device.

3D Printed Microfluidic elements

The different elements required by microfluidic devices printed with FFM will be looked at in turn. These include channels, mixers, reaction chambers (cavities), reservoirs (inlets), outlets, and connectors (hose barbs and threaded connectors).

Control of flow through the structures will be gravity driven (multiple steps can be initiated by device rotation). Gravity driven flow is simple and requires no external equipment. This work demonstrates that the "reaction-ware" technique (device rotation directs gravity flow through the device) to control a relatively sophisticated multi-step reaction sequence used by the sarin detection microfluidic device.

Study the fluid flow using gravity feed.

Gravitational flow rates were measured for tubes with different cross sections, lengths, and slopes. Two simple methods for quantifying the gravitational flow rate were employed – time to drain and time to fill. Time to drain (TTD) measures the time it takes for a given volume of liquid to drain from an inlet basin into an angled tube. Time to fill

(TTF) measures the time it takes to fill a cavity (reaction chamber), after passing through an angled tube. Examples of the Time to Fill and Time to Drain devices are shown in Figure 7.

To compensate for any initiation delays (time for the fluid to first reach the outlet basin for example) the flow rates were actually extracted from the slope of the flow volume versus time curves (see example in Figure 8). It was also necessary to add surfactant to the water to reduce the surface tension, otherwise with the small tube dimensions water sometimes would not flow into the tubes at all or would be delayed in starting to flow.

For the most part square cross sectional tubes were used so unless otherwise noted you can assume the tube had a square cross section. A tube designated as 2mm ID would have a 2mm x 2mm square cross section. One mm ID tubes were not consistently open, so there is limited data for devices with 1 mm ID tubes. One mm is approximately the resolution limit for the Lulzbot Mini using a 0.5mm nozzle.

Zhu et al introduced an analytic model for flow velocity in a channel with a rectangular cross-section[xi] (Zhu 2004):

$$\langle u \rangle = \frac{2}{3} U_{max}$$

$$U_{max} = \frac{gh^2}{8vl} H$$

where <u> is average flow velocity, U_{max} is the maximum velocity, g is the acceleration of gravity, h is the height of the channel, v is the kinematic viscosity of the solution, l is the length of the channel and H height difference between the inlet reservoir and the outlet.

Since h^2 is effectively the channel cross sectional area- A, H/l is sin(tube angle) or sin(θ), and g and v are constants we see that the flow rate is given by:

$$\langle u \rangle = constant \times \mathrm{A} \times \sin\theta$$

So that the flow rate for a tube is given by the cross sectional area and slope, independent of tube length.

Figure 9A shows curves for the water volume versus time to drain for tubes with ID ranging from 1mm to 3mm in 0.5mm increments and a 15° slope. It is evident the flow rate drops off rapidly as the tube ID decreases. If one looks at the flow density (flow rate divided by cross sectional area) through the tubes it is apparent that the flow density is not constant but falls off from 0.34 ml/mm2/sec for a 3mm ID tube to 0.05 ml/mm2/sec for a 1mm tube (Figure 9B). This would be consistent with a lower flow rate along the sidewall, thus the model does not accurately account for the flow difference due to tube cross sectional area.

The dependence of the flow rate on sin(θ), rather than the length of the tube, was verified by looking at the flow rate for tubes with the same cross sectional area and slope angle but with different lengths- 50mm and 100mm. The flow rate is independent of the tube length for a given tube angle (see Figure 9B), as predicted by the analytic model.

In Figure 10, the flow rate vs. sin(θ) is plotted for both the time to fill and time to drain structures. Both measurement techniques support the dependence of flow rate on sin(θ). In general the time to fill and time to drain measurements gave very similar results (see Figure 11B).

Circular tubes gave very similar results to square tube with the same cross sectional area (see Figure 11A).

Mixers: Testing Mixing efficacy

Because of the small dimensions used in microfluidics the fluid flow through the channels tends to be laminar, which makes mixing of fluid streams reliant on diffusion or on a channel design that disrupts the laminar flow. The Reynold's number for structures under consideration in this study is less than 1, which is well into the laminar flow regime (Re<2000 is considered laminar).

The efficacy of mixing for different structures will be measured qualitatively using dyes and quantitatively using pH. For the quantitative measurements, two liquids with different pH will be mixed in the microfluidic device (acetic acid and water), and the outflow from the mixer will be split. The pH of the two outflows will allow the calculation of the concentration of the acetic acid and subsequently to determine the mixing fraction.

An example of a simple T-mixer is shown in Figure 12. The two fluids, one acidic and one pH neutral, are simultaneously dispensed into the inlet basins which drain into the mixing junction and flow down through the angled tube, where the flow is separated in an outlet junction, flows out of the device, and is collected in beakers. The extent of mixing is evaluated by measuring the pH and calculating the concentration of acid that has been transferred from the acidic stream to the pH neutral stream. A blue and yellow dye was added to the two fluids to give a visual indication of the extent of mixing. The color of the outlet flows was compared to a series of known mixtures of the input fluids. This gave a quick indication of the relative mixing efficiency.

As a side note the ability to easily redesign and print new prototypes was helpful with the mixers. The outlet streams of the first mixers tended to flow along the base of the device making it impossible to completely capture the outlet flows. The devices were modified to add gaps underneath the outlet tubes to keep the flow from running along the bottom of the device.

A 0.72 molar acetic acid solution with a yellow dye was used for the first solution and water with a blue dye was used at the second solution. Since acetic acid is a weak acid the pH is not a direct measure of the acid concentration. It is necessary to calculate the concentration using the dissociation equation:

$$K_d = \frac{[H^+][CH_3OO^-]}{[CH_3COOH]}$$

Where $K_d = 1.75 \times 10^{-5}$ at room temperature (25°C).

Three different T-mixers were evaluated. Each had 2 x 2 mm inlet and outlet tubes and a 50mm 15° mixing tube which differed in the mixing tube interior:

Mixer 1: 3 x 3 mm tube

Mixer 2: 2 x 3 mm tube with baffles

Mixer 3: 2 x 2 mm tube (no baffles)

Pipette pumps were used to dispense 18ml of the liquids at equal rates into the inlet basins. Careful attention was paid to make sure the mixer was level so the 2 outlet flows were approximately the same and the pH changes were not due to a higher percentage of flow preferentially going to one of the outlets.

Mixer 1 and Mixer 3, which had no baffles in the mixing tube both showed incomplete mixing based on the pH of the outlet flows. By comparison the percentage of acetic acid in the two outlets from Mixer 2, which had baffles, was pretty much 50%,

ideal mixing. See the results in Figure 13. Comparing the colors of the two outlet mixtures, did indeed show that there was mixing but it was not possible to distinguish between 45% and 55% acetic acid concentrations.

Reaction Chambers: construction of cavities within the device

The formation of large cavities proved to be less of an issue than I thought it would be. The filament thread was able to successfully span a 40mm x 40mm cavity without sagging or breaking to form the "roof" of these structures. The key to success was that all 4 sidewalls provided support for the thread to anchor to. It could be problematic if there are large gaps along the top of the sidewalls. That situation is probably not very common and could be easily avoided by not putting inlets or outlets at the very top of a cavity. I didn't look at larger cavities since it's unlikely that larger cavities would be needed for microfluidics devices.

Construction of connectors

Designing a threaded connector is tricky. I had hoped to find designs on the web for pipe connectors but the ones I found were disappointing. A company called Orange Micro makes an Inventor add-in that can form many different types of standard threads, though they do not support NPT, which is the most common pipe thread in the US. I did print a few different threads using the ANSI 0.5-13 UNC standard size, both female and male successfully. The male and female parts did not readily join together. It may be that they would connect better with a metal fitting. On a side note there are a stunning number of thread standards available.

A barbed hose connector was easy to draw and printed well. Without supports the connector would need to come into the device from the top, rather than the side. This does not seem to be much of a limitation in microfluidic design since the direction of flow can easily be changed within the device by curving the channels/tubes.

Construction of a microfluidic Prototype for the detection of Sarin in blood samples

As a demonstration the utility of 3D printing in microfluidic prototyping the design and fabrication of a microfluidic device that could be used to detect Sarin gas in blood samples was undertaken. A similar devices was originally constructed using a multi-step soft lithography process[xii] (Tan 2008).

Device overview

This prototype sarin detection microfluidic device would measure the sarin concentration by observing the inactivation of AChE and subsequent slowdown of a chromophore reaction catalyzed by AChE.

The device consists of the microfluidic channels fabricated via 3D printing, filter media, F- inactivation media, bound AChE, and two glass slides to seal the device.

The flow within the device is gravity fed and controlled by rotating the structure by 90 degrees between 2 positions at each step of the process. A 3D drawing of the microfluidic device, along with a photo of the final device is shown in Figure 14.

The basic chemistry involved in the detection flow consists of 5 steps:

Sarin regeneration from the blood sample

Cell filtration and F- removal

AChE inactivation

Chromophore reaction (catalyzed by AChE)

Optical absorption measurement of the chromophore reaction.

The steps are outlined in Figure 15, along with the rotation of the microfluidic device used to move the chemicals from chamber to chamber.

Detailed look at the device operation

The first step mixes the blood sample containing sarin with an acidic sodium fluoride solution in a T-mixer that feeds into the sarin regeneration chamber (see Figure 16). An acidic solution of sodium fluoride (NaF) is used to release sarin from the AChE on the red blood cells[xiii] (Heilbronn 1965). With a NaF concentration of $5x10^{-3}$M and a pH of 5.0 approximately 90% of the sarin will be regenerated in 20 minutes.

During this step acetylthiocholine and DTNB (5,5-dithio-bis-2-nitrobenzoic acid) are mixed in the second T-mixer and drain into the chromophore reaction chamber, where AChE bound to beads catalyzes the reaction converting DTNB (colorless) to TNB (yellow) (see Figure 17). This serves as a reference for the extent of the AChE inactivation due to sarin contained in the blood sample.

In the second step the device is rotated 90° causing the sample to flow through the filter chamber removing the blood cells, platelets and other solids, and into the F- removal chamber. It is necessary to remove the F- to allow the sarin to bind to the AChE in the next step.

Also in step 2 the reference chromophore reaction is transferred to the optical absorption chamber. The TNB (2-Nitro-5-sulfanylbenzoic acid) chromophore product absorbs light at 412nm. A light source is attached to the glass slide at one end of the

absorption chamber and a detector is attached to the glass slide on the other end of the absorption chamber (see Figure 18).

In the third step the microfluidic device is rotated back to position one transferring the sarin containing blood sample to the chromophore reaction chamber which contains the bound AChE. The extent of AChE inactivation will depend on the concentration of sarin in the sample.

While this is happening the reference chromophore reaction solution drains out of the optical absorption chamber and out of the microfluidic device (see Figure 19).

In the fourth step the microfluidic device is rotated back to position 2. This drains the sarin containing sample out of the chromophore reaction chamber (see Figure 20). The microfluidic device is then rotated back to position 1 and the chromophore reactants are added into the chamber containing the AChE that has been inactivated by the sarin in the blood sample.

Finally, in step 5 the microfluidic device is rotated to position 2, transferring the chromophore reactants to the optical absorption chamber (see Figure 21). The absorption of the reaction with the inactive AChE is compared to the absorption of the reference reaction to estimate the sarin concentration (via the extent of AChE inactivation).

Chapter 4

Discussion

Today's typical desktop FFM 3D printer is capable of printing microfluidic channels just below 1mm in diameter which makes them suitable for some microfluidic applications. The ability to print with a wide variety of materials with different chemical resistance is attractive for microfluidics.

Gravity flow can be used to control the flow rate and the movement of liquids from one chamber to the next, allowing relatively complex chemical reaction sequences to be performed, as demonstrated with the gravity flow controlled sarin blood sample detection microfluidic device.

Gravity flow for smaller channel devices is hampered by the surface tension of water, which can prevent the flow from initiating in the device. Surfactants are necessary to make the flow more consistent. Smaller channels are more problematic than larger ones for gravity flow. For an application where a precise flow is required pumps may be needed.

3D design for 3D printing has a pretty substantial learning curve and careful consideration must be made to design supports for the object while it prints. Some rules (guidelines) were established to aid in the design of a successful print. Looking at the slices used to generate the print can be helpful for finding weaknesses in the support of a design.

If you’re willing to commit to the initial learning curve, the ability to rapidly design and print microfluidic prototypes or specialty devices makes 3D printing with FFM a very affordable and versatile option.

Figures

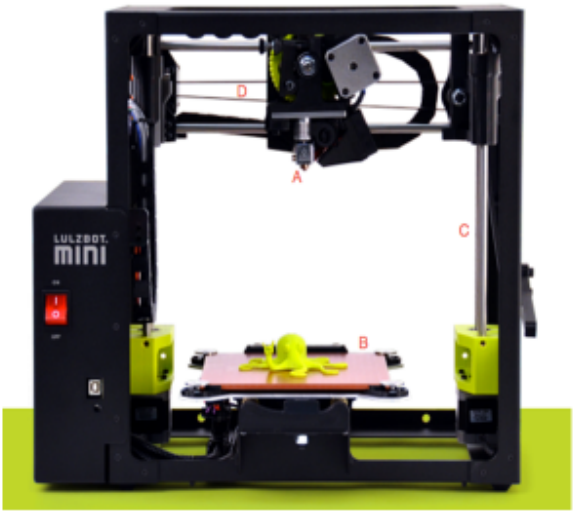

Figure 1: Lulzbot Mini FFF 3D printer. Key components include the nozzle (A), build platform/stage (B), z positioning rail (C), and the x positioning pulley (D).

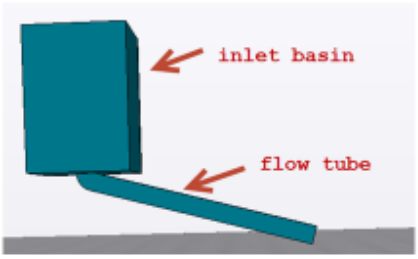

A) STL view – 3D view

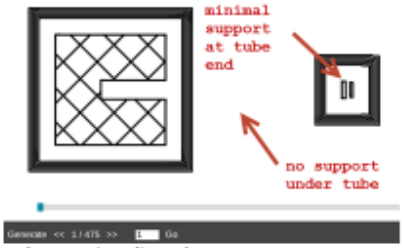

B) First Slice (base)

C) Support fails during print

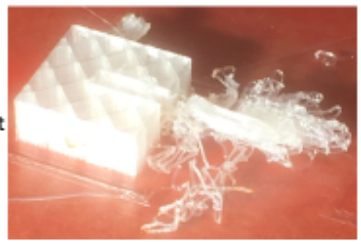

Figure 2: Time to Drain device with auto-generated support. Software failed to provide sufficient support for the device to print successfully. Tiny contact area with the print stage at the tip of the flow tube and no support under most of the flow tube led to failure.

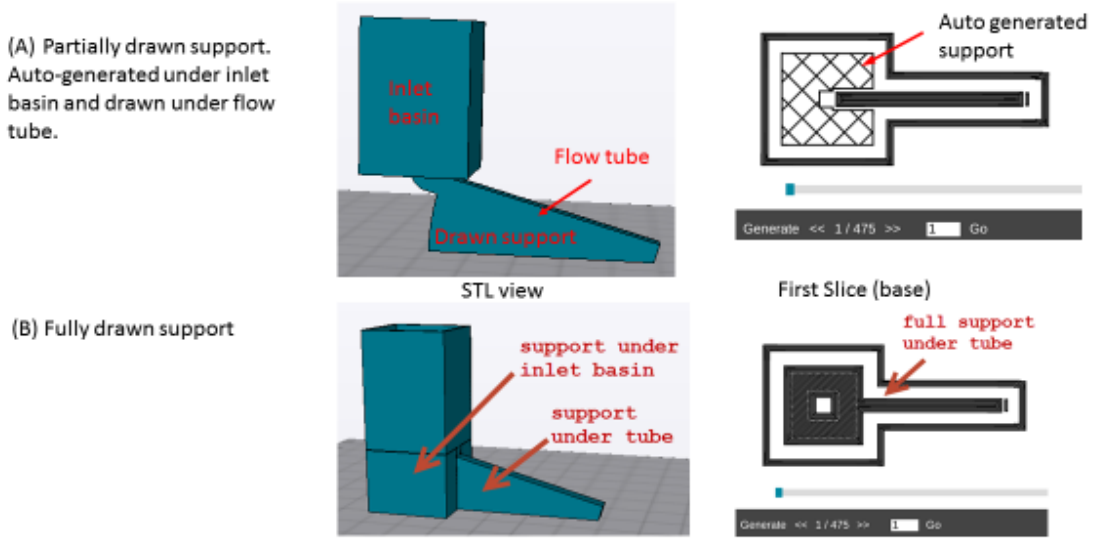

Figure 3: Partially drawn and fully drawn supports for Time to Drain Structure

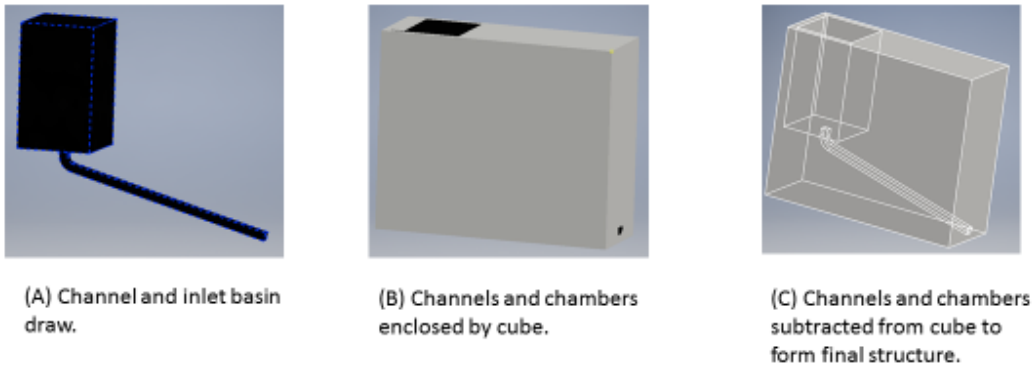

Figure 4: Alternate Design Technique for a Time to Drain Structure. Microfluidic chambers and channels are drawn (A), enclosed by a cube (B), and then subtracted from the cube to form the final structure. While the design effort was less, the print time increased from 3hr 44min (structure shown in Figure 3) to over 11 hours.

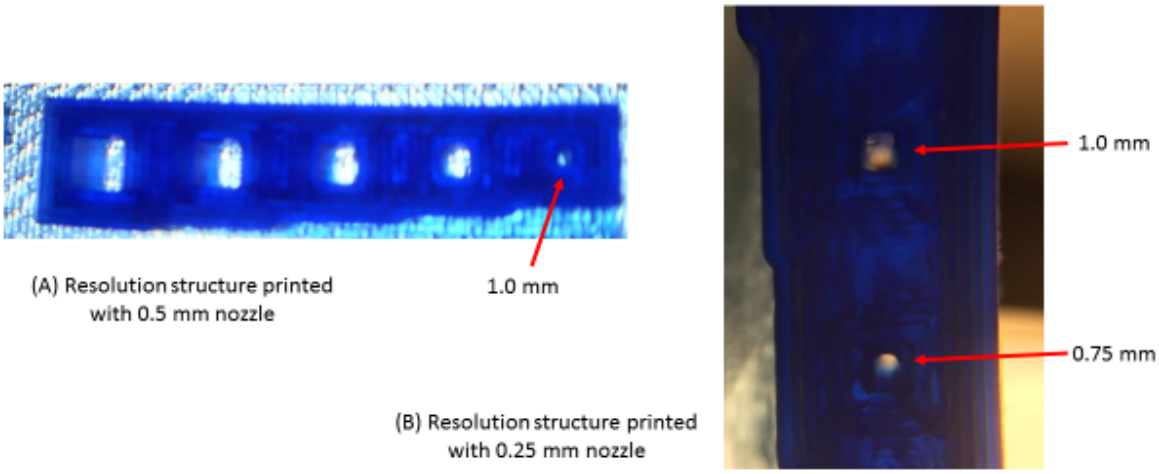

Figure 5: Resolution structures. Resolution structure with 0.5mm nozzle. Tubes range from 3.0mm to 1.0mm in 0.5mm increments (L->R). (B) Resolution structure printed with sub mm features using a 0.25mm nozzle.

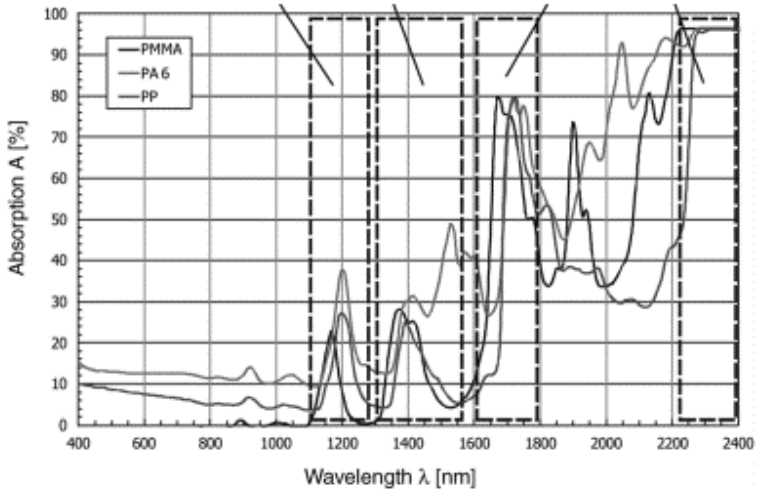

Figure 6: Absorption spectra of PMMA, PA6, and PP (polypropylene). From Laser Welding of Plastics, 1st Edition, Rolf Klein. 2011 Wiley-VHC Verlag GmbH

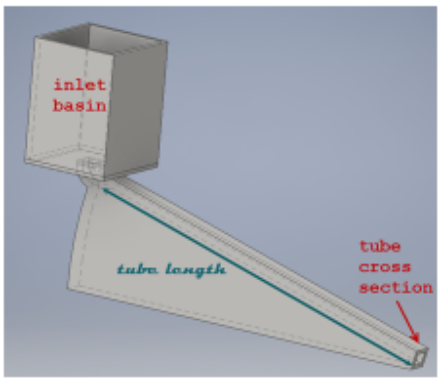

Time to drain (TTD)

Varying volumes of liquid added to inlet basin and time to drain into tube was recorded.

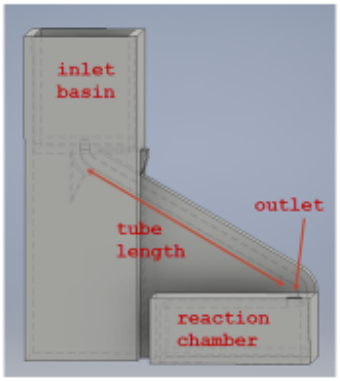

Time to fill (TTF)

Excess volume of liquid added to inlet basin and time to fill the reaction chamber of fixed volume is recorded.

Figure 7: Time to Drain and Time to Fill Flow rate structure

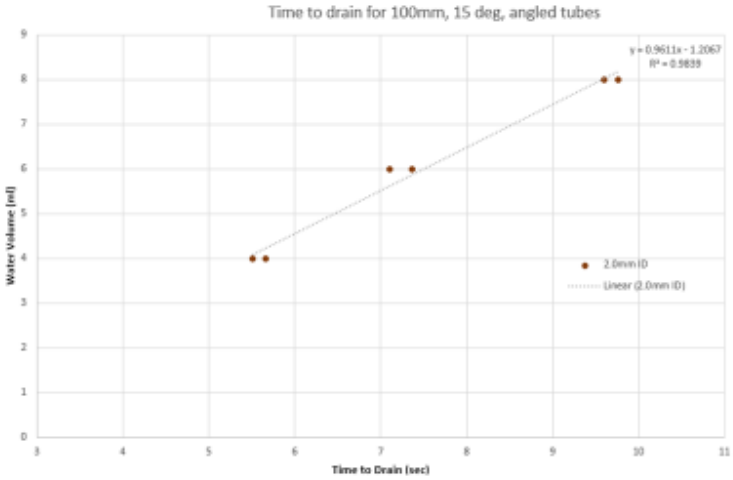

Figure 8: Flow Rate extraction

Flow rate extracted from the slope of the water volume vs. time to drain curve.

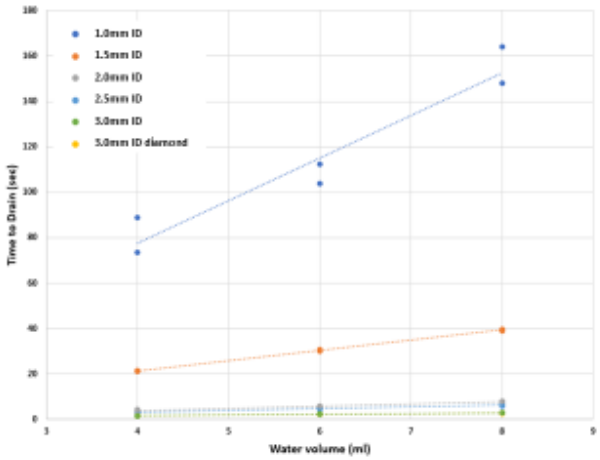

(A) Time to Drain for 50mm, 15° angled tubes

length	ID	flow rate ml/sec	cross section (mm^2)	Flow Density $ml/mm^2/sec$
50	1.0	0.05	1	0.05
	1.5	0.22	2.25	0.10
	2.0	1.03	4	0.26
	2.5	1.19	6.25	0.19
	3.0	3.13	9	0.35
	3.0	3.09	9	0.34
100	1.5	0.15	2.25	0.07
	2.0	0.98	4	0.24
	2.5	1.54	6.25	0.25
	3.0	3.46	9	0.38

(B) Time to Drain flow rates and flow density for 50mm and 100mm, 15° angled tubes

Figure 9: Time to Drain measurements for 15° Angled Tubes. Note that flow density drops off for smaller tubes and flow rate is independent of tube length.

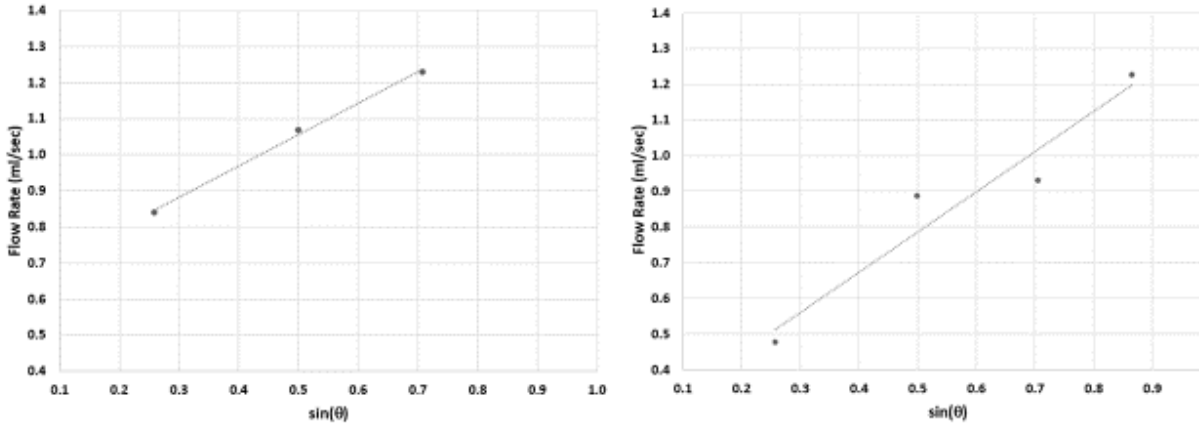

(A) Time to fill data

(B) Time to drain data

Figure 10: Flow Rate vs. sin(θ). For 50mm long, ID=2mm tubes . Both Time to Fill (TTF) and Time to Drain (TTD) data support the model's flow rate dependence on sin(θ),

			Flow Rates	
X-section (mm2)	ID	radius	square tube	circular tube
4.00	2.0	1.13	1.03	1.03
6.25	2.5	1.41	1.19	1.54
9.00	3.0	1.69	3.13	3.08

(A) Flow rates with circular and square tubes

ID (mm)	Angle	TTD	TTF
2	15	1.03	0.84
3	15	3.13	2.89
2	30	0.88	1.07
2	45	0.93	1.23

(B) Flow rates as measured by TTF and TTD

Figure 11:Comparing flow rates. (A)Comparing square and circular tunes with the same cross sectional area. (B)Comparing Time to Fill and Time to Drain measurements.

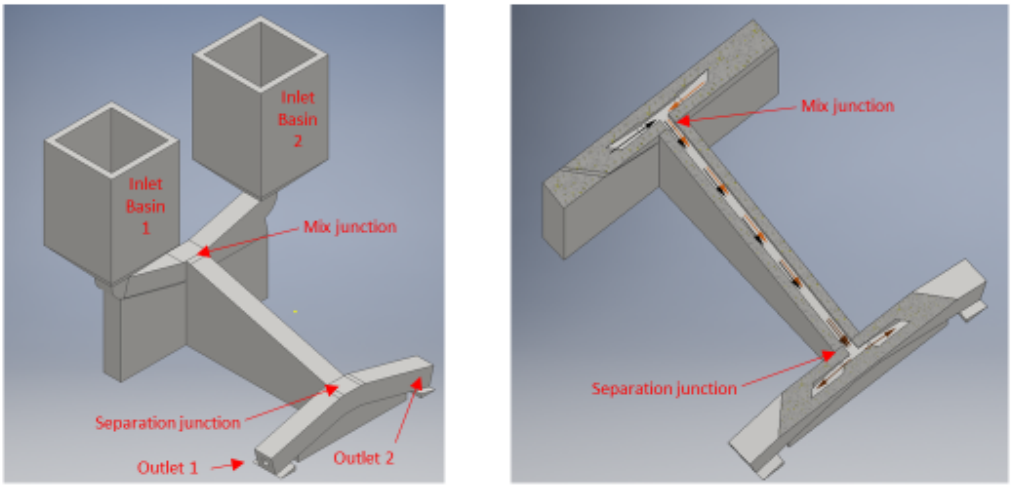

Figure 12: T- mixer Drawings. (A)3D Drawing. (B)Cross section through mix tube

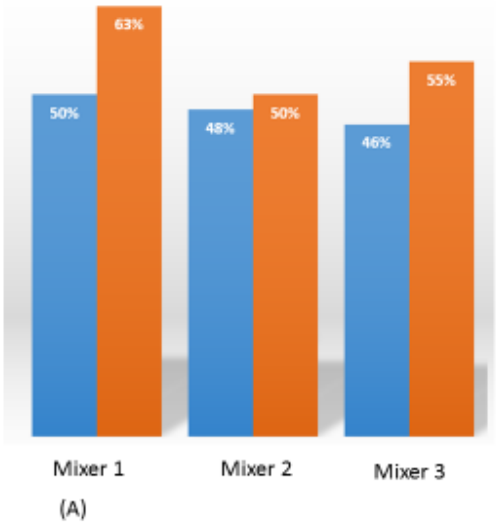

	Acetic acid molarity	pH
Acetic acid input	0.723	2.45
Water input	0	7.30
50-50 mix	0.363	2.60
Mixer 1 outlet 1	0.363	2.6
Mixer 1 outlet 2	0.457	2.55
Mixer 2 outlet 1	0.347	2.61
Mixer 2 outlet 2	0.363	2.6
Mixer 3 outlet 1	0.331	2.62
Mixer 3 outlet 2	0.398	2.58

(B)

Figure 13: Mixer results. (A)Bar chart showing % acetic acid in each mixer outlet. (B)Tabular data for mixer results

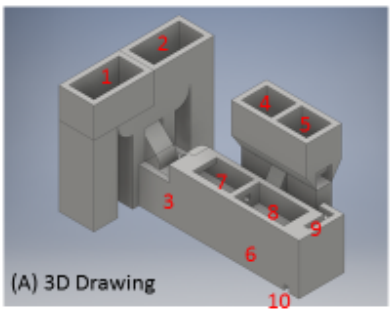

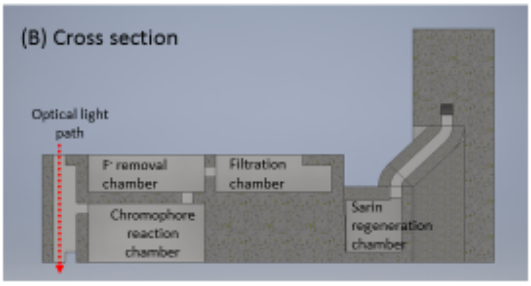

1. Blood Inlet Basin
2. NaF Inlet Basin
3. Sarin release chamber (not visible)
4. DTNB inlet basin
5. Acetylthiocholine inlet basin
6. Chromophore reaction chamber with AChE catalyst (not visible)
7. Filtration chamber
8. F⁻ removal chamber
9. Optical Absorption port
10. Fluid outlet

(B) 3D Printed Device

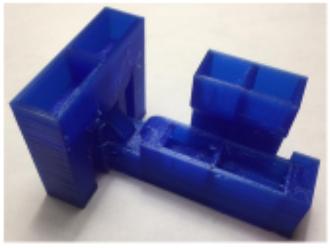

Figure 14: Sarin detection microfluidic device

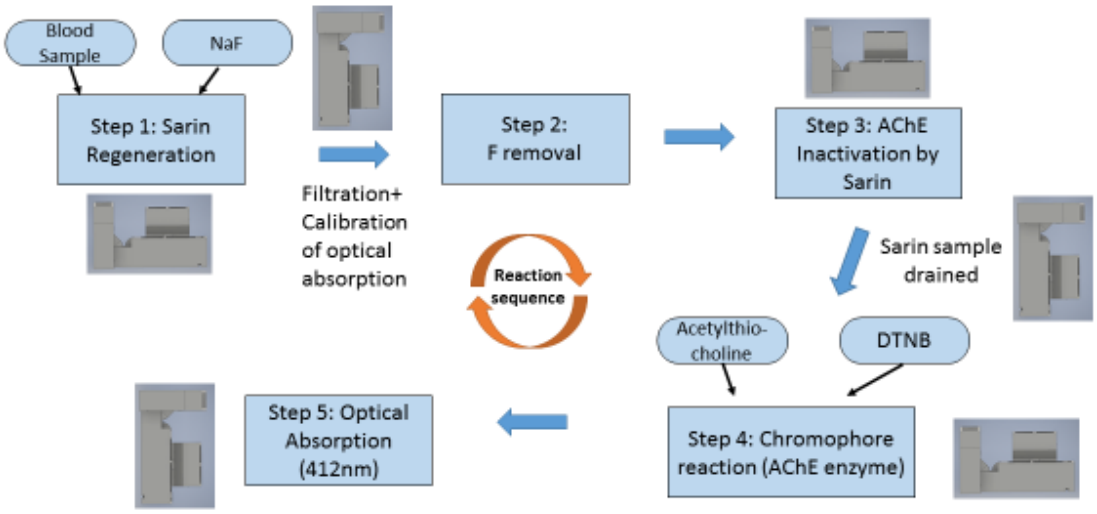

Figure 15: Chemical reaction sequence underlying sarin detection in the microfluidic device. Also shown is the rotation of the microfluidic device, which moves chemicals from chamber to chamber for different steps of the process.

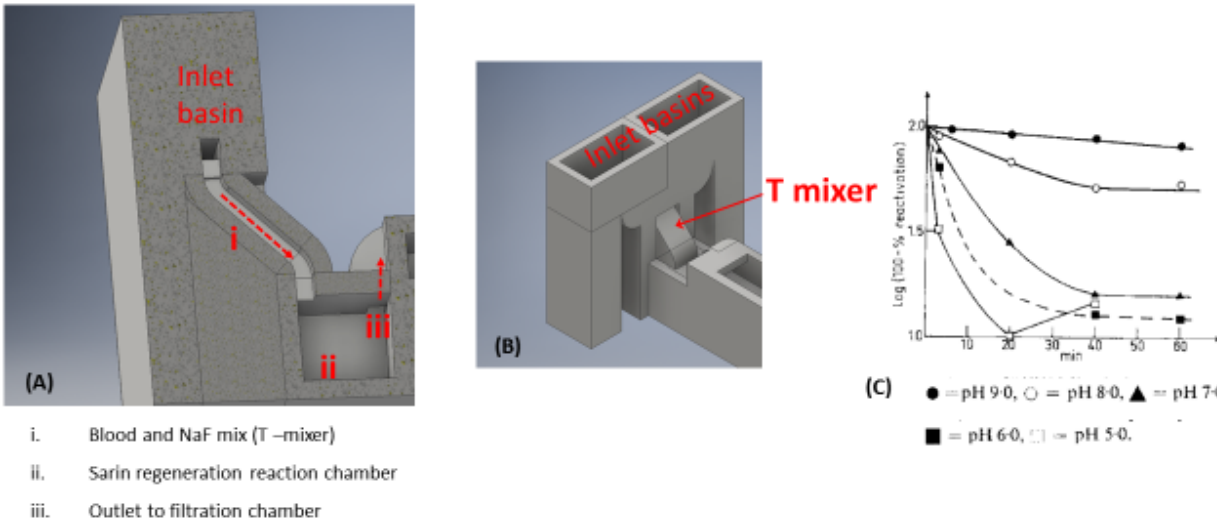

Figure 16: Sarin regeneration from blood sample. (A) Blood Sample is mixed with an acidic NaF solution. Cross section of mix tube leading into regeneration chamber. (B)External 3D view. (C)Sarin regeneration in acidic NaF solutions

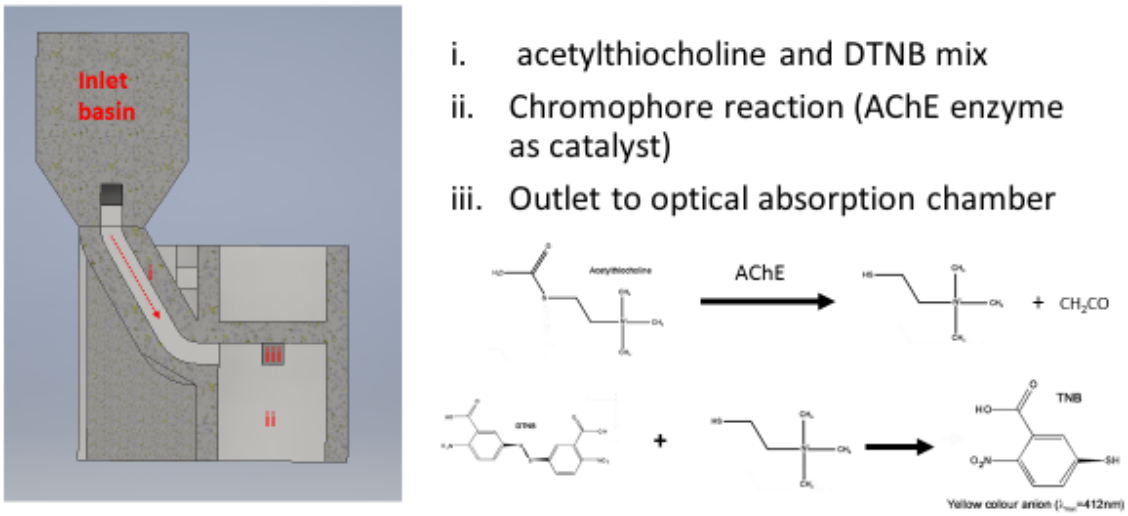

Figure 17: Baseline chromophore reaction. AChE is active, giving a baseline reading for comparison with the AChE inactivation later on. This is happening in parallel with the sarin regeneration.

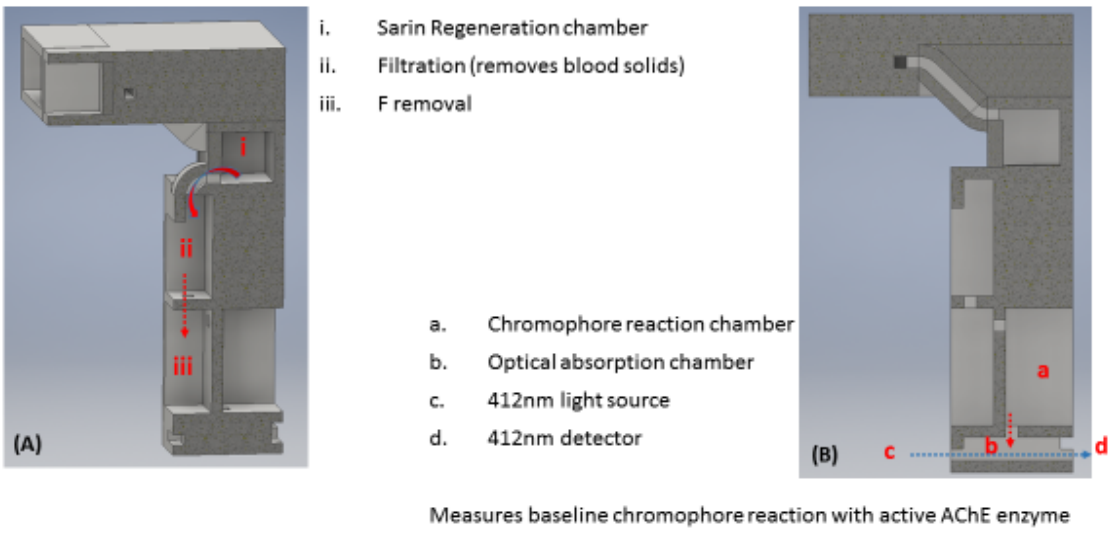

Figure 18: Filtration and F- removal. (A)Filtration and F- removal from blood sample (B)Baseline chromophore reaction absorption measurement

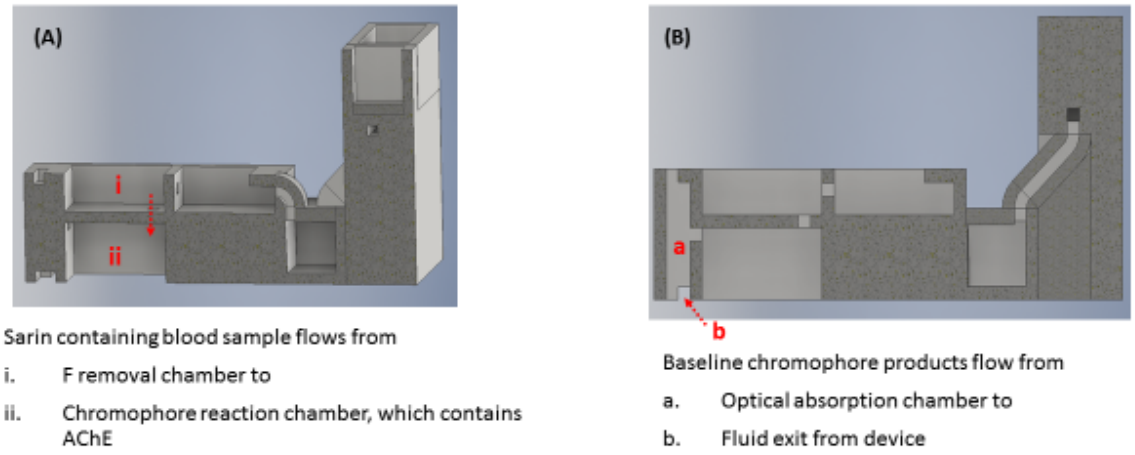

Figure 19: AChE inactivation. Blood sample flows into chromophore reaction chamber (contains AChE). Baseline chromophore reation is drained from the device

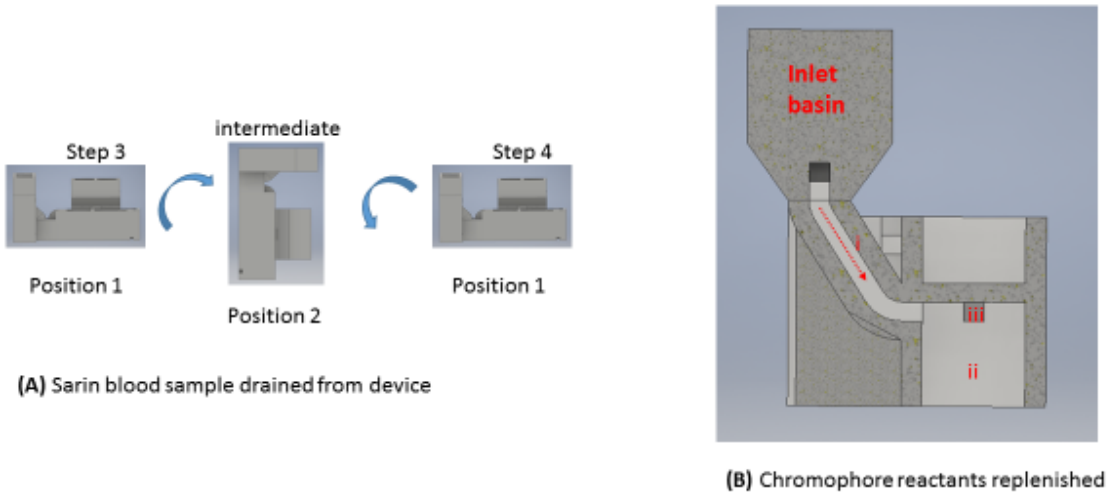

Figure 20: Chromophore reaction with inactivated AChE. (A)Series of rotations drains sarin from the device. (B)Chromophore reaction replenished in chromophore reaction chamber (containing inactivated AChE)

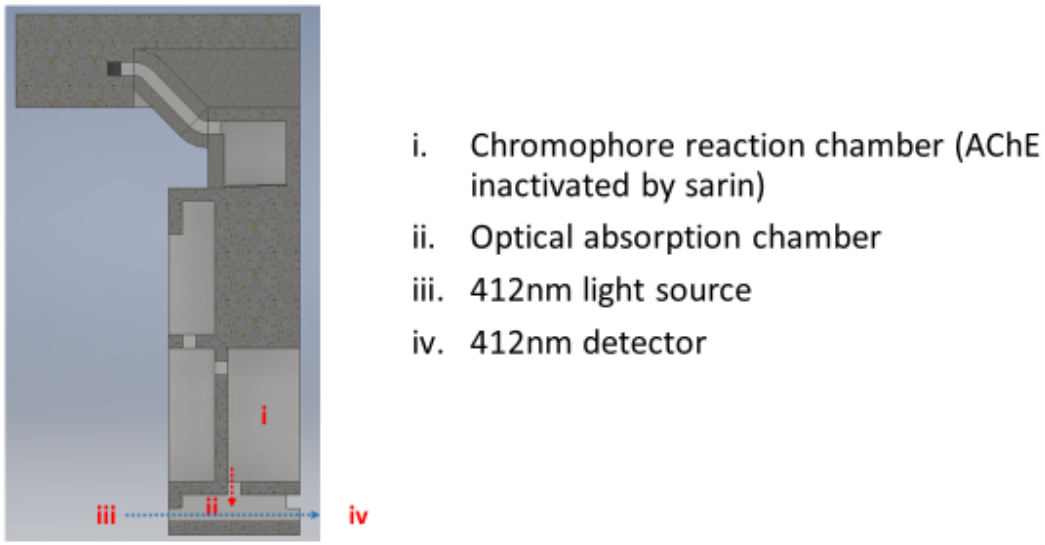

Figure 21: Final Step – chromophore absorption measured. Last rotation moves chromophore products to the optical absorption chamber. Absorbance compared to reference reaction performed earlier.

References

[i] Streets, A.M. & Huang, Y. (2013). Chip in a lab: Microfluidics for next generation life science research. Biomicrofluidics **7**, 011302.

[ii] Whitesides, G. M., Ostuni, E., Takayama, S., Jiang, X. & Ingber, D. E. (2001). Soft Lithography in Biology and Biochemistry, Annual Review Biomed. Eng., 3, 335–373.

[iii] Martinez, A.W., Phillips, S.T., Butte, M.J., & Whitesides, G.M., (2007). Patterned Paper as a Platform for Inexpensive, Low-Volume, Portable Bioassays. Angew. Chem. Int. Ed., 46, 1318 –1320.

[iv] Hiemenz,J. (2014) White Paper: 3D PRINTING WITH FDM. Retrieved from: http://usglobalimages.stratasys.com/Main/Files/White%20Papers/WP_FDM_3D%20PrintingWithFDM.pdf?v=635786177472811876

[v] Gross,B.C., Erkal, J.L., Lockwood, S.Y., Chengpeng Chen, C., & Spence, D.M. (2014). Evaluation of 3D Printing and Its Potential Impact on Biotechnology and the Chemical Sciences. Analytical Chemistry, 86, 3240−3253.

[vi] Ansgar Waldbaur, Holger Rapp, Kerstin Lange, & Bastian E. Rapp (2011). Let there be chip—towards rapid prototyping of microfluidic devices: one-step manufacturing processes. Analytic Methods, 3, 2681-2716.

[vii] Wang,H., Masood, S., Iovenitti, P., & Harvey, E. (2001). Application of Fused Deposition Modelling Rapid Prototyping System to the Development of Microchannels. BioMEMS and Smart Nanostructures Proceedings of SPIE Vol. 4590, 213-220.

[viii] Bishop, G.W., Satterwhite, J.E., Bhakta, S., Kadimisetty, K., Gillette, K.M., Chen, E., & Rusling J.F (2015). 3D-Printed Fluidic Devices for Nanoparticle Preparation and Flow-Injection Amperometry Using Integrated Prussian Blue Nanoparticle-Modified Electrodes. Analytical Chemistry, 5 *87* (10), 5437–5443.

[ix] Kitson, P.J., Symes, M.D., Dragone, V., & Cronin, L. (2013). Combining 3D printing and liquid handling to produce user-friendly reactionware for chemical synthesis and purification. Chem. Sci., 4, 3099-3103.

[x] Khorasani,M.T., Mirsadeh, H., & Sammes, P.G. (1999). Laser Surface modification of polymers to improve biocompatibility: HEMA grafted PDMS. Radiation Physics and Chemistry, Vol.55(5), 685-689.

[xi] Zhu, X., Chu, L.Y., Chueh,B., Shen, M., Hazarika,B., Phadkea, N., & Takayama, S. (2004). Arrays of horizontally-oriented mini-reservoirs generate steady microfluidic flows for continuous perfusion cell culture and gradient generation. Analyst , 129 , 1026–1031.

[xii] Tan, H., Loke, W., Tana, Y., & Nguyen, N. (2008). A lab-on-a-chip for detection of nerve agent Sarin in blood. Lab Chip, 8, 885–891.

[xiii] Heilbronn, E. (1965). Action of Fluoride on Cholinesterase-II. In Vitro reactivation of cholinesterases inhibited by organophosphorous compounds. Biochemical Pharmacology, Vol. 14, 1363-1373.